END
DATE
FILMED
11-81
DTIC

REPORT DOCUMENTATION PAGE	READ INSTRUCTIONS BEFORE COMPLETING FORM

1. REPORT NUMBER	2. GOVT ACCESSION NO.	3. RECIPIENT'S CATALOG NUMBER
NRL Memorandum Report 4657	AD-A106 230	

4. TITLE (and Subtitle)	5. TYPE OF REPORT & PERIOD COVERED
THE OROGRAPHIC EFFECTS INDUCED BY AN ISLAND MOUNTAIN RANGE ON PROPAGATING TROPICAL CYCLONES	Interim report on a continuing NRL problem.
	6. PERFORMING ORG. REPORT NUMBER

7. AUTHOR(s)	8. CONTRACT OR GRANT NUMBER(s)
S. W. Chang* and R. V. Madala	

9. PERFORMING ORGANIZATION NAME AND ADDRESS	10. PROGRAM ELEMENT, PROJECT, TASK AREA & WORK UNIT NUMBERS
Naval Research Laboratory Washington, DC 20375	61153N; RR033242; 43-0909-A-1

11. CONTROLLING OFFICE NAME AND ADDRESS	12. REPORT DATE
Office of Naval Research Arlington, VA 22217	October 30, 1981
	13. NUMBER OF PAGES
	48

14. MONITORING AGENCY NAME & ADDRESS(if different from Controlling Office)	15. SECURITY CLASS. (of this report)
	UNCLASSIFIED
	15a. DECLASSIFICATION/DOWNGRADING SCHEDULE

16. DISTRIBUTION STATEMENT (of this Report)

Approved for public release; distribution unlimited.

17. DISTRIBUTION STATEMENT (of the abstract entered in Block 20, if different from Report)

18. SUPPLEMENTARY NOTES

*Present address: Science Applications, Inc., McLean, VA 22102

19. KEY WORDS (Continue on reverse side if necessary and identify by block number)

Tropical cyclone
Mountain effect
Tropical meteorology

20. ABSTRACT (Continue on reverse side if necessary and identify by block number)

Numerical simulations with a primitive equation model and parameterized physics are conducted to study the orographic effects on translating tropical cyclones induced by an island mountain range. The model has 51 × 51 horizontal grid points with 60 km resolution and seven σ-layers in the vertical. The idealized topography with 2000-m peak is introduced over a 12-h growth period. The initial state contains a gradiently balanced vortex embedded in a uniform, unsheared tropical easterly flow.

(Continues)

DD FORM 1473 EDITION OF 1 NOV 65 IS OBSOLETE
1 JAN 73
S/N 0102-014-6601

20. ABSTRACT (Continued)

Many orographic effects are produced similar to that observed for typhoons passing over Taiwan. The storm tends to translate at about twice the speed of the basic flow near the mountain, while its intensity is reduced. Air flows mostly around the mountain range instead of over it, forming a ridge on the windside and a trough on the leeside slopes. The disturbed flow produced a mean cyclonic circulation around the mountain. Therefore, the model tropical cyclone makes a cyclonic curvature in its path around the north end of the island mountain in its path.

Further numerical experiments demonstrate that cumulus heating forces the cyclonic circulation around the mountain. We found that the lower level circulation of an unforced, quasibarotropic vortex is blocked by the mountain range. Instead, secondary low-level circulation center forms in the induced lee trough. The secondary low-level center develops as the upper level center becomes a phase.

A vorticity budget is performed for the 700-mb airflow just before the landfall. It confirms the importance of diabatic processes in producing the observed orographic effects. Diabatic processes generate convergence to maintain the vorticity of the tropical cyclone. The horizontal advection of positive vorticity in conjunction with the leeside vortex stretching, results in the mean positive vorticity around the topography.

CONTENTS

DTIC
SELECTED
OCT 27 1981
B

THE OROGRAPHIC EFFECTS INDUCED BY AN ISLAND MOUNTAIN RANGE
ON PROPAGATING TROPICAL CYCLONES

1. INTRODUCTION

The island of Taiwan, with its Central Mountain Range (CMR)
soaring up to more than 3000 m at only 50 km from its eastern sea
shore (Fig. 1), induces many interesting topographic effects on
the weather. In winter, the northeasterly monsoon winds travel
unobstructedly over the kuroshio and produce prolonged periods of
rain over most of the northern and eastern parts of the island.
In summer, the northwestern Pacific high pressure system is in
control and the weather is highlighted by frequent typhoons. As
typhoons approach the island, their behavior can be influenced
substantially by the high CMR.

Brand and Blelloch (1974) found that westward traveling
typhoons tended to move cyclonically around the northern side of the
CMR (Fig. 1). The average translation speed changed from 8 m s^{-1} 48 h
before the landfall to 12 m s^{-1} at the landfall. Noticeable weak-
ening started 12 h prior to the landfall. Chu, Wang and Pao (1977) showed
by streamline analysis some detailed flow structures such as flow
separation and vortex shedding associated with the typhoon circula-
tion around the island. Wang (1980) has compiled so far the most
complete data of 53 typhoons that came close to Taiwan between
1946-1975. He documented of these typhoons their paths, intensities,
propagating speeds and life histories. He found that some typhoons
passed over the island by taking a cyclonic track similar to those
described in Brand and Blelloch. There were, however, some other
cases where typhoons passed over the island by forming a secondary
circulation center to the leeside so that the storm tracks were not
continuous.

The observed behavior of typhoons has been reproduced in laboratory experiments (Chang and Chen, 1969; Pao and Hwang, 1977; Wei, 1979). Unfortunately, neither quantitative analyses nor physical insights in understanding the mechanism of the island-induced effects were given.

This study is to investigate the physical mechanisms involved in the observed behavior by numerical simulations with an idealized topography. We will discuss in the following Sections 2 and 3, respectively, the numerical model and the incorporation of the idealized topography to the model. The orographic effects of the island mountain range on an approaching tropical cyclone will be discussed in Section 4. We will examine in Sections 5 and 6, the effects of cumulus convection and surface friction on tropical cyclones moving over a mountain range. A vorticity budget will be given in Section 7 to explain the observed cyclonic movement of the typhoons near the CMR.

2. **THE NUMERICAL MODEL**

The problem of the air flow over an isolated mountain is a very interesting one in fluid dynamics as well as in weather forecasting. In earlier mathematical models (see Smith, 1979 for review), the case of stratified, rotating, barotropic basic fluid over mountain, whose surface coincides with an isentropic surface, is considered. The solution of such a quasi-geostrophic approach is

2

that the flow near the mountain is similar in its structure to the classical description of a cold-core anticyclone. The maximum vertical displacement of the isentropic surfaces decreases with height, but the horizontal extent of the lifting increases with height (see e. g. Bussi and Tibaldi, 1977). Thus, quite different from the simple conservation of potential vorticity, an air column approaching the mountain would undergo a stretch before the mountain elevation due to the lifting of the stream surfaces, a contraction over the mountain, and then a stretch after passing the mountain.

It is very difficult to find a meteorological situation that fits the foregoing discussion, because those solutions are pertinent only to large scale ($\sim$ 1000 km) mountains. For the mesoscale mountains under consideration where the Rossby number (Ro) approaches 1, the quasi-geostrophic assumption breaks down and inertial effects must be included. Merkine and Kalnay-Rivas (1976) used the semi-geostrophic approximation (Merkine, 1975) to study the rotating stratified flow around finite, isolated topography. They found the flow consists of a topographically-bounded anticyclonic vortex. The vortex is baroclinic near the mountain and barotropic far away from the mountain. The anticyclonic vortex intensifies the velocity field on the left-hand side of the mountain (facing downwind) and decreases it on the right hand side. They also found from

trajectory analysis that all trajectories possess cyclonic curvature over the mountain. The cyclonic curvature must be accompanied at higher elevation by anticyclonic shear in order to be consistent with the conservation of potential vorticity. Buzzi and Tibaldi (1977) obtained a similar solution using an expansion in powers of Ro to solve for the flow in an unbounded fluid. The semi-geostrophic solution remains symmetric about the topographic axis perpendicular to the flow. Bussi and Tibaldi stated that the semi-geostrophic assumption is still too restrictive to describe tne propagation of inertial gravity waves, especially when Ro increases to or exceeds unity.

Hayes and Williams (1977) used an inviscid, adiabatic, primitive equation (PE) model to study the steady, unsheared flow past a finite large scale mountain range. Their results indicated that the mountain induces a pressure ridge over the mountain and a low level trough on the leeside. They showed further that the results are insensitive to the vertical resolution of the model if the horizontal resolution is sufficient. The horizontal resolution affects the fine scale features of the flow. Recently, Tibaldi, Bussi and Malguzzi (1980) investigated the orographic effects of the Alps on an approaching baroclinic wave with a PE model. They found that a small scale baroclinic process caused an amplification of the initial disturbance produced by the mountain when the large scale wave passed over it.

4

In our present study of a diabatically-forced tropical cyclone interacting with a mesoscale mountain, an initial value, PE model seems most appropriate. The numerical model we used is identical to the one in Chang and Madala (1980).

a.   Governing Equations

The governing equations are in pressure-weighted flux form for conservations of momentum, temperature, and water vapor. The normalized pressure P/p_s ($= \sigma$) is the vertical coordinate. The system is assumed hydrostatic.

b.   Physical Parameterizations

A boundary layer parameterization based on a generalized similarity theory (Chang, 1981) is employed. The surface layer logarithmic-linear profiles are matched with the mixed layer profiles so that only one model layer is needed to represent the boundary layer. The relevant universal functions of stability A, B, C and D are formulated according to Yamada (1976). The surface roughness length over the ocean surface are computed following Charnock's equation,

$$z_o = C \, u_*^2 \, / \, g \qquad\qquad (1)$$

5

The roughness over the mountain is assumed to be a linear function
of elevation

$$Z_o = 1 + 0.0005 \times h_s \qquad cm \qquad (2)$$

We note that the PBL over rugged mountain surface under high
wind conditions may not be well modeled by our parameterization. One
shortcoming is the assumption of constant PBL height. The PBL
parameterication is nevertheless applied in the expectation that the
similarity theory in general will still hold under these conditions.

A simplified version of Anthes' (1977) cumulus parameterization
is utilized. The total latent heating is determined by vertical
integration of water vapor convergence, which occurs mainly in the
boundary layer. Vertical distribution of latent heating depends on
the conditional instability. The vertically averaged relative humidity
(RH) regulates the partition of latent heating and moistening. Large
scale ascending motion in a saturated environment results in the
release of latent heat on the resolvable scale.

c.   Initial Conditions and Boundary Conditions

The mean hurricane sounding (Sheets, 1969) is used for the
initial thermodynamic state. The lapse rate is conditionally

6

unstable from the surface to about 350 mb and the RH is high up to 500 mb. The initial flow field is a uniform, unsheared easterly current at a speed of 5 m s^{-1}.

The initial vortex embedded in the easterly flow is non-divergent with tangential velocities described by

$$v_o (r) = v_{max} \frac{r}{r_{max}} \exp. \left\{ \frac{1}{2} \left[1 - \left(\frac{r}{r_{max}} \right)^2 \right] \right\} \qquad (3)$$

where the maximum tangential velocity v_{max} is 16 m s^{-1} at a radius of r_{max} = 210 km from the storm center. The surface pressure and temperature fields are obtained by a non-linear, non-divergent initialization method, and are in gradient balance with the flow field.

The Neumann lateral boundary conditions are applied to all variables. Sponge boundary conditions are imposed at the inflow and outflow boundaries to prevent bounding reflection. The non-dimensional diffusion coefficients $K_H (\Delta t) (\Delta x)^{-2}$ there are $\sim O(10^{-3})$, which are one order of magnitude larger than those in the interior.

d.   Model Structure

The model atmosphere from P_s to $P = 0$ is divided into seven
sigma layers as in Chang and Madala (1980). The sigma layers are
bounded by $\sigma = 0$, 0.1, 0.2, 0.35, 0.55, 0.77, 0.93, and 1. All
variables except $\dot{\sigma}$, the vertical velocity, are defined at the center
of each layer and $\dot{\sigma}$ is defined at the boundary of each layer.
The momentum points and mass points are fully staggered in horizontal
direction following the scheme C in Arakawa and Lamb (1981).

The horizontal resolution is uniformly 60 km throughout the
model domain. The model domain is 3000 x 3000 km (51 x 51 grid
points) so that the movement of the vortex is not affected by the
lateral boundaries over the period of integration.

The spatial differencing is second-order accurate and conserves
mass, mementum, and enthalpy. The split-explicit method (Madala, 1981)
is applied for temporal integration.

3.   The Idealized Topography

The idealized topography (Fig. 2) is used to represent the
terrain of Taiwan. Due to the horizontal resolution of the model, some
of the details in the topography shown in Fig. 1 are smoothed out. The

8

idealized topography has an east-west extent of 240 km and north-south extent of 480 km (Fig. 2a). Fig. 2 also shows the east-west cross-section AB (Fig. 2b) and north-south cross section CD (Fig. 2c). The idealized terrain is symmetric about its ridge.

The topography is introduced by a linear growth from 0-12 h, because a dynamically balanced initial state with the orographic effects is unknown. The maximum surface pressure change at the ridge is ~18 mb h^{-1} during the switch-on period. A quasi-steady flow is established by 24 h, with surface pressure tendency less than 0.3 mb h^{-1} anywhere in the model. The switch-on of the mountain causes a surface pressure increase of ~1 mb over the flat region. A similar technique to introduce a mountain has been utilized in Hayes and Williams (1977) and Tibaldi et al (1980).

To test the sensitivitiy of the numerical solution to the mountain switch-on, we have conducted several supplementary experiments with a uniform, unsheared, straight basic flow. The effects of cumulus convection and surface friction were suppressed for these experiments. First we varied the switch-on period. No significant difference was found in the quasi-steady solutions among the cases whose switch-on periods vary from 8-24 h. We also varied the size and height of the topography. It was found the details of the flow were sensitive to the characteristics of the mountain. But there

was a trend in the variations and the large features in the flow
were persistent. We thus conclude that the idealized topography
and the method to introduce it are adequate.

The reaction of the basic uniform, unsheared flow to the
idealized topography is of course very interesting by itself. Since
there is no vertical wind shear in the basic flow, there is little
evidence of mountain waves. The surface flow pattern is quite different
from that at higher levels. The surface flow is highly anticyclonic,
with much of the mass flowing around the south side of the mountain due
to its blocking effect. There is a wake of low wind speed on the leeside
until the northern branch and the stronger southern branch converge at
250 km west of the ridge. At 700 mb, the flow is still anticyclonic around
the mountain with a leeside trough. There is little branching of the
flow to either side of the mountain. Overall, the mountain-induced
perturbation at 700 mb is smaller than that at the surface.

4.   Orographic Effects on the Translating Vortex

Several numerical integrations were carried out to isolate
different physical processes. Table 1 lists all the experiments.

Table 1

List of All Experiments

Experiment	Characteristics
1	No topography
2	Topogrpahy
3	Topography, No Cumulus Heating
4	Topography, No Surface Friction

Experiment 1 contains no topography. The tropical cyclone in the experiment reaches quasi-steady state at 24 h with central pressure of 978 mb and maximum wind of 32 m s^{-1}. Its path is approximately 5° to the right of the mean easterly flow, similar to the result of Chang and Madala (1980). The mean translating speed is that of the ambient mean flow. In this section we focus on the comparison of Exps. 1 and 2.

a.   **Intensity and Path**

The central pressure of Exp. 2 is never lower than 988 mb, which is 10 mb weaker than Exp. 1. The central pressure of 988 mb is

reached at 24 h and stays with $\pm$ 2 mb until 54 h when the integration
is terminated. The maximum surface wind is greatly affected by
the mountain, it reaches 32 m s^{-1} at 18 h, decreasing to 22 m s $^{-1}$
just before the landfall (Fig. 3). But as the center of the
circulation moves past the topography, the storm regains it
strength, the maximum wind increases to 26 m s^{-1}. The decrease
of maximum winds as typhoons pass Taiwan is clearly illustrated in
Brand and Blelloch (1974).

The mountain has great influence on the translating speed
and path of the cyclone. We learned that the tropical cyclones travel
over ocean surface with a mean path approximately 5° to the right
of the basic current and a mean speed close to that of the basic
current (Chang and Madala, 1980; also, Exp. 1). However, in Exp. 2,
the translation speed of the tropical cyclone increases as it
approaches the mountain to 10 m s^{-1} (Fig. 4) as compared to the speed
of the basic flow of 5 m s^{-1}. After the storm center passes the
ridge, a sudden deceleration takes place. By 54 h, the translation
speed decreases to ~3 m s^{-1}.

Because of the positive static stability, the air in the lower
troposphere tends to travel around the mountains instead of over it.
When the storm center is located to the east of the range, a stronger

12

easterly flow is formed to the north side of the mountain, whereas
the westerly wind south of the center is turned into southerly.
This cyclonic circulation in the lower troposphere around the
mountain not only speeds up the storm but also causes the storm to
move north to the east of the mountain (Fig. 6) and south to the west
of the mountain.

The changes in speed and the curvature in the path of the
storm are in agreement with observations (cf. Fig. 1).

b.   Circulation

The wind vector and vorticity at 36, 42, 48 and 54 h at the
700 mb and the surface levels are shown in Fig. 5 and 6. At the
700 mb level, the circular wind field near the center remains nearly
intact as the storm passes over the mountain ridge. The easterly
flow north of the island is much stronger than the flow to the south,
which turns from westerly at 36 h to southerly at 48 h. The vorticity
field indicate that the vorticity is in general cyclonic in the
northern part of the island mountain because of its proximity to
the storm. The vorticity is in general cyclonic everywhere except
on the windside in the southern part of the mountain where it is
anticyclonic. A secondary center at the southern tip of the island
exists briefly around 36 h but it has no significant consequences.

13

The flow at the surface level ($\sigma = 0.965$) is more complex.
The circular wind field near the storm center is deformed, and the
vorticity contours stretch along the ridge. Due to the orographic
obstruction, there is very little wind component normal to the ridge,
air tends to flow around the mountain. This results in a sharp
turning of airflow on the windside slope and a wake of low speed on
the leeside slope.

At 42 h, when the center is located near the ridge, the
airflow around the center is disorganized, and the maximum vorticity
associated with the storm is reduced. Secondary low at southern tip
of the mountain exists from 36-42 h. Convergence of air into the
main center is evident throughout the period. At 54 h, the circular
wind field near the center is reorganized, and the vorticity field
had regained its intensity.

As mentioned before the path of the storm has a cyclonic
curvature induced by circulation around the mountain. The storm's
fast translation speed between 36 and 48 h is also due to its northerly
shift into the stronger easterly to the north of the mountain. The
circulation of the surface layer, defined as

$$C = \oint u\ dx + v\ dy \quad , \qquad\qquad (4)$$

integrated counterclockwisely around a 480 km x 720 km rectangular box centered around point D in Figure 2, is computed (Fig. 7). The surface level circulation is about -4×10^{10} cm^{2}s^{-1} at 24 h. It rapidly increased with time to $+18 \sim 20 \times 10^{10}$ cm^2 s^{-1} at 40 hr, indicating a strong cyclonic flow around the terrain.

To further demonstrate the strong easterly around the north side, the rate of mass flows defined as

$$M(x) = - \frac{1}{g} \int_1^{0.5} \int_y P_s(x,y) \, u \, (x,y,\sigma) \, dy \, d\sigma \qquad (5)$$

are computed. The quantity M represents the rate of westward mass flow across a vertical cross-section at certain longitude bounded by $\sigma = 0.5$ and 1.

Fig. 8 shows the values of $M(x)$ for the cross-section from the northerm tip of the island to the northern model boundary (solid line) and the cross-section from the southern tip of the island to the southern model boundary (dashed line). Since the basic flow is uniform, the values of the two $M(x)$ are equal at $\sim 2.8 \times 10^{13}$ g along the lateral inflow boundary. During the period 24 h $\sim$ 48 h, the northern $M(x)$ increases to $5 \sim 6 \times 10^{13}$ g, while the southern

M(x) decreases to 1×10^{13} g or even negative values indicating a
reversed (eastward) mass flow there.

It is evident from these results that the mountain has
significant influence on the propagating tropical cyclones. The
terrain induces a low-level cyclonic circulation around the mountain,
and diverts most of the easterly mass flow to the north of the
terrain. Thus the storm center is forced to move cyclonically
about the mountain into the strong easterly flow there and results
in its fast movement across the mountain. The mountain weakens the
circulation by practically blocking the airflow at the low levels.

c.   <u>Vertical Velocity and Precipitation</u>

The topography has strong effects on the vertical velocity
field, the low-level upward motion mainly occurs on the windside
slopes. As evidence by the $\omega(=dp/dt)$ field at $\sigma = 0.97$ (Fig. 9),
the peak upward motion at 36 h occurs in the region to the north of
the storm center and over the northern part of the island, where the
wind direction is in land (see Fig. 6). At 42 h, the region with the
upward motion is widespread, but mainly restricted to the northern
part of the mountain range where wind speed is high. At 48 h, the strong
upward motion is shifted to the windslopes in the south of the mountain.

The upward motion at PBL top is well correlated with precipitation, which is responsible for most of the typhoon damage. The real precipitation distribution of course is more complicated due to the complex terrain and the large scale distribution of specific humidity. The distributions shown in Fig. 9 construct only a general picture, because the initial specific humidity field in the model is assumed uniform.

5.   The Effect of Latent Heat Released in Connective Clouds

To determine the effect of the release of latent heating by the cumulus convection, we integrated the numerical model with the diabatic heating and the surface friction terms suppressed (Exp. 3). Without there two effects, we effectively eliminate the possibility for the initial vortex to intensify. Indeed, the vortex experiences a gradual weakening throughout the integration due to internal friction.

The movement of the low-level vortex center and the airflow around the mountain in Exp. 3 are notably different from those in Exp. 2. The original westbound surface vortex center (Fig. 10) decelerates between 36 and 48 h as it approaches the mountain and shifts northward. It stops at the location denoted by 60 h east of the mountain. It dissipates completely by 72 h. As the original vortex is dissipating, a surface secondary center appears at 36 h at the southern tip of the mountain and moves slowly northward.

17

At 60 h, another surface secondary center occurs 300 km to the west. In the mean time, the 700 mb center passes the ridge at the speed of the basic current, taking a slightly anticyclonic trajectory. The secondary center develops and becomes the major surface center as the upper level center aligns vertically with it over the open sea after 72 h.

There is a strong easterly airflow with anticyclonic vorticity to the south of the mountains in the surface flow (Fig. 11). This anticyclonic low with minimum vorticity to the southeast of the mountain, extends northward, deforms the vortex, and shifts the vortex center northward. The wake to the west of the ridge, characterized by low wind speeds, contains return flows and secondary center. The upper airflows (not shown) are similar to those in Exp. 2 (Fig. 5) except for the anticyclonic curvature in the path of the vortex.

The low-level circulation around the terrain (computed by Eq. 4, plotted in Fig. 7) is predominantly anticyclonic at $-8 \sim -10 \times 10^{-10} \text{ cm}^2 \text{ s}^{-1}$, except for a brief period ~ 60 h. Even then, the maximum value is no more than $2 \times 10^{10} \text{ cm}^2 \text{ s}^{-1}$. The values of M(x) (defined by Eq. 5, plotted in Fig 8) show much less north-to-south polarization compared with Exp. 2 due to the presence of the stronger easterly surface flow to the south and the absence of the strong easterly flow to the north.

The momentum field in Exp. 3 is decoupled vertically, the wind shear between the surface level and upper level is unrealistically large. Exp. 3 of course cannot represent any real situation because there is always vertical coupling due to convection and turbulence. However, according to Wang's (1980) classification, there are typhoons that passed Taiwan's CMR (Type I, several examples are shown in Fig. 1) and there are those that were blocked by CMR and reformed from secondary center (Type II). Figure 12 shows some type II cases. Table 2 shows that the intensities of types I and II before the landfalls are quite different. The mean central pressure of type I is 30 mb lower than type II, the mean maximum wind of type I is $\sim$18 m s^{-1} stronger than type II. The observed typhoons are more intense than our simulation mainly because of the horizontal resolution in our model. We have performed further tests on the resolution problem and the results are presented in the Appendix.

It is conceivable that there are stronger cumulus convection and better vertical structural coherence in strong typhoons than weak typhoons. Our experiments suggest that intensity is a deciding factor in tropical cyclone's behavior in passing high mountain range. Strong cyclones pass with modifications and weak cyclones are disturbed to a large extend with their low-level circulations blocked.

TABLE 2

Intensities of Two Types of Typhoons Passing Taiwan

Type	Number of Cases	Mean Central Pressure (Standard Deviation)	Mean Maximum Wind (Standard Deviation)
I	22	949 mb (23.8)	52.4 $m\ s^{-1}$ (9.0)
II	12	979 mb (12.7)	36.8 $m\ s^{-1}$ (12.6)

We thus conclude that the latent heating by cumulus convection plays an important role in the tropical cyclone's reaction to the topography. The latent heating keeps the circular wind field relatively intact in spite of the orographic obstruction. It produces a stronger easterly flow to the right side (relative to the storm track) of the mountain with cyclonic circulation. Such airflow field produces a fast translation speed and a cyclonic movement of the storm center as shown by Fig. 1. The lack of latent heating results in the weakening of the storm. When encountering the mountain range, weak tropical cyclones tend to form low-level anticyclonic circulation around the mountain and develop leeside secondary center.

6. Effect of Surface Friction

Exp. 4 is conducted with the cumulus parameterization suppressed. A comparison of Exps. 3 and 4 shall indicate the effect of the surface friction. The behavior the vortex in Exp. 4 is very similar to that in Exp. 3 in the vortex's translation speed, path and flow pattern at high levels. The surface flow in Exp. 4 is weaker than that in Exp. 3 as expected. The original vortex is hardly identifiable at 48 h, the secondary center is also less well defined. The weak circulation is illustrated by Fig. 7.

We should note that Exp. 4 again does not represent any realistic situation. The surface friction, which dissipates kinetic energy, produces energy-generating cross-isobaric flow. The frictionally-induced convergency further enhances the cumulus convection in conditionally unstable atmosphere. However, Exp. 4 points out that the surface friction, over either the mountain or the ocean, does not contribute directly to the particular behavior of a tropical cyclone passing over a mountain.

7. Vorticity Budget

It is useful for field forecasters to estimate from a simplified vorticity budget the circulation (or mean vorticity) around the island mountain when a typhoon approaches. Neglecting the dissipation for the time being, one can approximate the absolute vorticity tendency following an air volume by

$$\frac{d}{dt} (\zeta + f) = - (\zeta + f) \, \nabla \cdot \underset{\sim}{V} = - (\zeta + f) (\nabla \cdot \underset{\sim}{V})_o - (\zeta + f) (\nabla \cdot \underset{\sim}{V})_d \qquad (6)$$

where $(\nabla \cdot \underset{\sim}{V})_o$ is the orographically-induced divergence and $(\nabla \cdot \underset{\sim}{V})_d$ is the divergence generated by diabatic processes in the storm. To maintain the obsolute vorticity in the air volume, one needs

$$-(\nabla \cdot \underset{\sim}{V})_d \geq (\nabla \cdot \underset{\sim}{V})_o \qquad (7)$$

22

Suppose air flows completely over the mountain at mid-troposphere
the orographically-induced divergency on the windside slope can
be expressed for first-order approximation as

$$(\nabla \cdot \underset{\sim}{V})_o \sim \frac{V_n}{gH}\left(\frac{\partial \phi_o}{\partial x}\right) \qquad (8)$$

where V_n is a typical wind speed normal to the mountail range near
a tropical cyclone, H is the scale height. Expression $\frac{1}{g}\left(\frac{\partial \phi_o}{\partial x}\right)$
is the slope of the mountain, and is equal to 0.0167 for
the idealized topography. Let $V_n = 25 \text{ m s}^{-1}$ and $H = 8$ km, we get
$-(\nabla \cdot \underset{\sim}{V})_d \leq -5 \times 10^{-5} \text{ s}^{-1}$, which is equivalent to a cumulus
heating rate of $\sim 110 \text{ }^{\circ}K \text{ day}^{-1}$ or precipitation rate of
$\sim 35 \text{ cm day}^{-1}$. This means that the divergence induced by our
idealized topography is equivalent in magnitude to the convergence
in a fairly strong tropical system. In a quasi-steady tropical
cyclone, the vorticity generated by $-(\nabla \cdot \underset{\sim}{V})_d$ is nearly balanced
by internal dissipation and surface friction. By obtaining $(\nabla \cdot \underset{\sim}{V})_o$
from (8), one can estimate the rate of exponential decay in time of a
storm's vorticity by integrating a simplified vorticity equation.

In reality, the vorticity budget is more complex than the
disscusion above. Having a three-dimensional model, we can
diagnose the contribution to vorticity generation of each term in
the vorticity equation.

The vorticity equation in pressure-coordinates can be written
as (Holton, 1979)

$$\frac{\partial \zeta}{\partial t} = - \underset{\sim}{V} \cdot \underset{\sim}{\nabla} (\zeta + f) - \omega \frac{\partial \zeta}{\partial p} - (\zeta + f) \underset{\sim}{\nabla} \cdot \underset{\sim}{V} + \hat{k} \cdot (\frac{\partial \underset{\sim}{V}}{\partial p} \times \underset{\sim}{\nabla} \omega) + S \quad (9)$$

$$\quad\quad\quad (I) \quad\quad\quad\quad (II) \quad\quad (III) \quad\quad\quad\quad (IV) \quad\quad\quad (V)$$

where symbols have their conventional meterorological meanings.
The terms on the right represents, respectively, the effects of
horizontal advection, vertical advection, divergence, twisting,
and sink or source due to diabatic processes. The last term
is mainly due to friction and diffusion in our model, it should
be proportional to the value of the vorticity due to the physical
parameterization in our model. The characteristic scales pertinent for
our present study are $U \sim 5$ m s^{-1}, $W \sim 10$ mb h^{-1}, $L \sim 200$ km, $\Delta p \sim$
100 mb and $f = 5 \times 10^{-5}$ s^{-1}. A straightforward scale analysis
gives orders of magnitude for the terms: term I ~ 0 (10^{-9}),
term II ~ 0 (10^{-9}), term III ~ 0 (10^{-8}), and term IV ~ 0 (10^{-9}).
The magnitude of term V is difficult to estimate for the
problem under investigation, it should be equal to or less than the
magnitude of term I or III. Therefore, unlike the large scale flow,
the effects of twisting and divergence are far from negligible in
the vorticity budget for this mesoscale problem.

Because the cyclonic circulation around the mountain
grows rapidly between 24 to 48 h (Fig. 7) and the surface pressure
at the peak is about 800 mb, we selected the 700 mb flow at
36 h (Fig. 5) for vorticity budget study. In order to make
use of Eq. (9), model data are linearly interpolated to isobaric
surfaces. Vertical differences are taken over a 150 mb thickness.
It turns out that the contribution of vertical advection is small.
The distributions of terms I, III and IV are shown in Fig. 13.
We note that the 36 h vorticity field (Fig. 5a) consists of
strong cyclonic vorticity near the center and to the leeside
slopes, and anticyclonic vorticity on the windside slopes. The
contribution to local vorticity change due to horizontal advection
(Fig. 13a) is approximately 1/4 wavelength out of phase downwind
from the vorticity field. The strong positive tendency between the
ridge and the storm center in conjunction with the positive tendency
downwind from the leeside trough, contributed to the formation of
the discussed cyclonic circulation around the mountain (Fig. 7)
at this time.

There is negative tendency in the distribution of term III
(Fig. 13b) over the windside slopes and positive tendency over the
leeside slopes due to vortex stretching. The positive tendency
northwest to the storm center is apparently associated with the
tropical cyclone itself. The high wind speed and cumulus con-
vections in the front-and-right quadrant produces a strong

convergence there, and hence the positive tendency. This positive
tendency maintains a strong vorticity near the storm center, which
in turn produces the distribution of term I due to horizontal
advection. In Exp. 3, where cumulus convection and surface
frictin is suppressed, this region of positive tendency is
conspicuously absent. Note also that the center of the positive
tendency region is located north of the storm center, this is a
symptom of the northward movement of the center. There is another
maximum positive tendency to the south of the mountain associated
with the secondary center (see Fig. 6a).

The twisting term (term IV) is confined to the mountainous
region. It indicates that only in this region a horizontal
differential of vertical motion is coupled with a vertical wind
shear and that the flow near the mountain is highly baroclinic.

Again we find in the vorticity budget that the diabatic
effects play an important role in producing the orographic effect.
The diabatic processes generate convergence near the center of the
tropical cyclone to maintain its vorticity field, which by
horizontal advection, causes a cyclonic circulation around the
island mountain.

8.　Summary and Discussion

The orography effects on propagating tropical cyclone
exerted by an idealized mesoscale, island mountain range was
investigated by using a multi-layer PE model with parameterized physics.
The numerical simulation successfully reporduces the following
observed behavior of the westward propagation tropical cyclones:
(1) The intensity of the tropical cyclone is reduced; (2) the
translating speed increases before passing the mountain ridge;
(3) the storm center moves cyclonically in passing over the mountain;
(4) the distribution of vertical motion is orographically
modulated, upward motion occurs on the windside slopes where
the vorticity is positive.

The results indicated that the approaching tropical
cyclone induces a cyclonic circulation around the topography.
The mountain range constitutes a physical obstruction to the
low-level flow and generates a strong easterly mass flow to the
north of the mountain range.

Further experiments showed that the strong latent
heating by cumulus convection is responsible for the generation

of the above mentioned cyclonic circulation. In the experiment without cumulus heating, the circulation around the mountain is mostly anticyclonic, and the low-level vortex center is blocked by the mountain range. Secondary vortex centers form in the lee trough and develop when in phase with the upper level vortex center. These experiments helped explain the observed different behavior of weak typhoons from that of stronger ones.

The important role of the diabatic effects was confirmed by a vorticity budget study on the flow before the landfall. It is the convergence generated by the cumulus heating and surface friction that produces a strong vorticity field. The positive vorticity advection in front of the storm compensates the negative vorticity tendency due to vortex compression on the windside slope, and, in conjunction with the vortex stretching on the leeside, results in a positive mean vorticity over the mountain range.

Our numerical model can of course be improved. The major shortcomings are related to the PBL formulation over the mountain and the horizontal resolution. We may have stretched the model's PBL parameterization in applying it over rugged mountain terrains under windy conditions. A multilevel PBL

formulation is perhaps needed in spite of the cost. The 60 km resolution in our model is only marginally acceptable for the storm (see Appendix). A nested grid system can help circumvent the problem at not much greater expense.

Many of our conclusions cannot be substantiated due to a lack of indepth analyses of observation data. Case studies as well as composite studies on existing data are needed to further advance our understanding of the tropical cyclone's behavior in crossing mountain ranges.

ACKNOWLEDGMENT
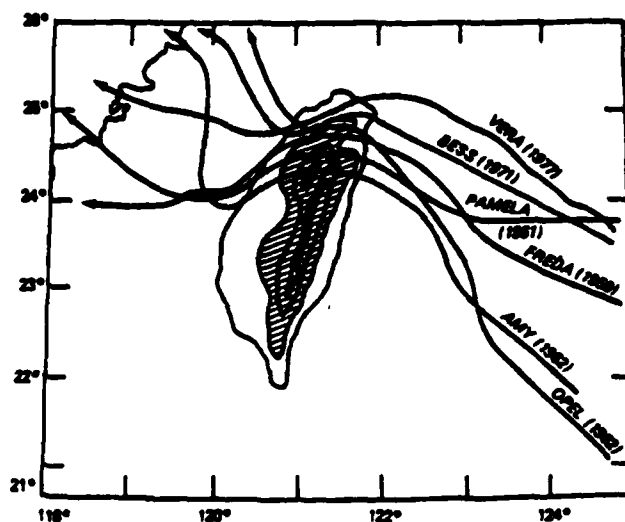
Fig. 1 — The Terrain of Taiwan and paths of some typhoons. The contours, plotted every 1000 m, are simplified.
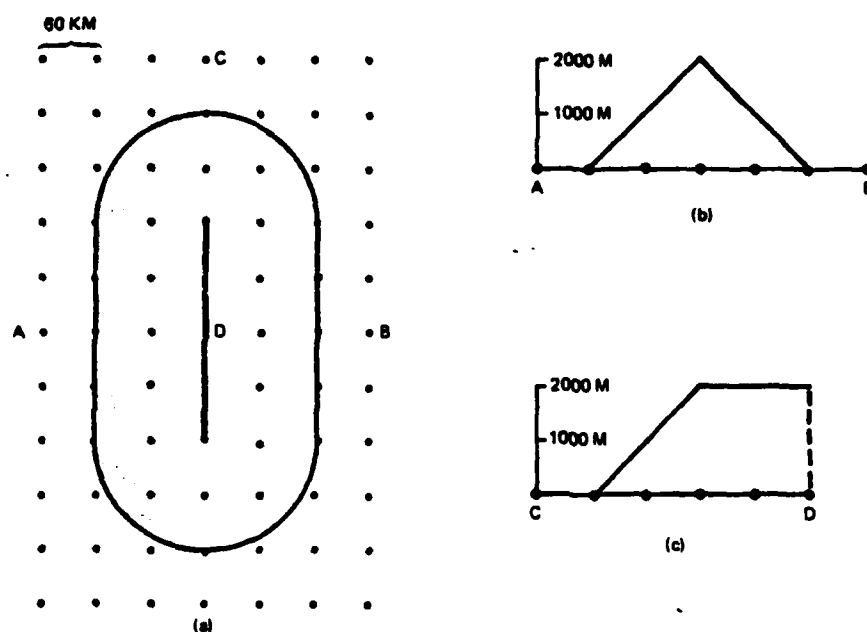
Fig. 2 — The idealized topography: (a) a plan view, shaded regions are elevated; the dark line in the center represents the ridge; dots are model grid points; (b) a northward view of the AB cross-section; (c) an eastward view of the CD cross-section.
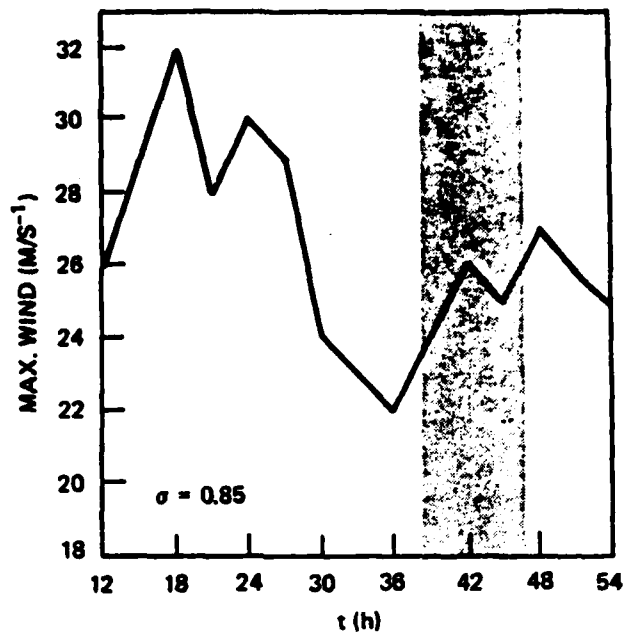
Fig. 3 — The temporal variations of the maximum surface wind of Exp. 2. The shaded area denotes the time the strom center is over the land.
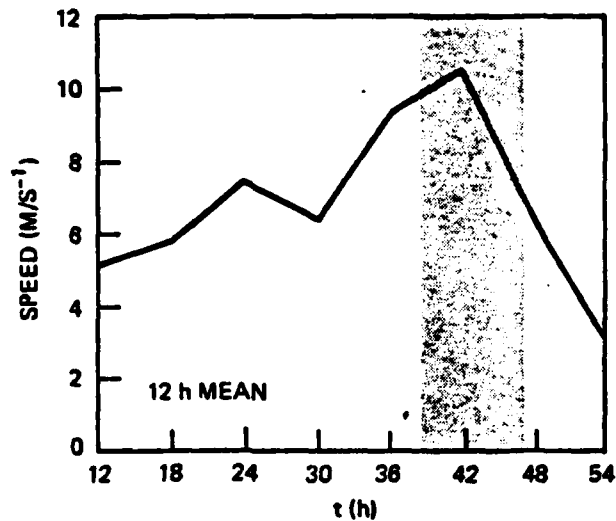
Fig. 4 — Same as Fig. 3 except for the 6-h average translating speed. Note the speed of basic flow is ~5 ms $^{-1}$.

31
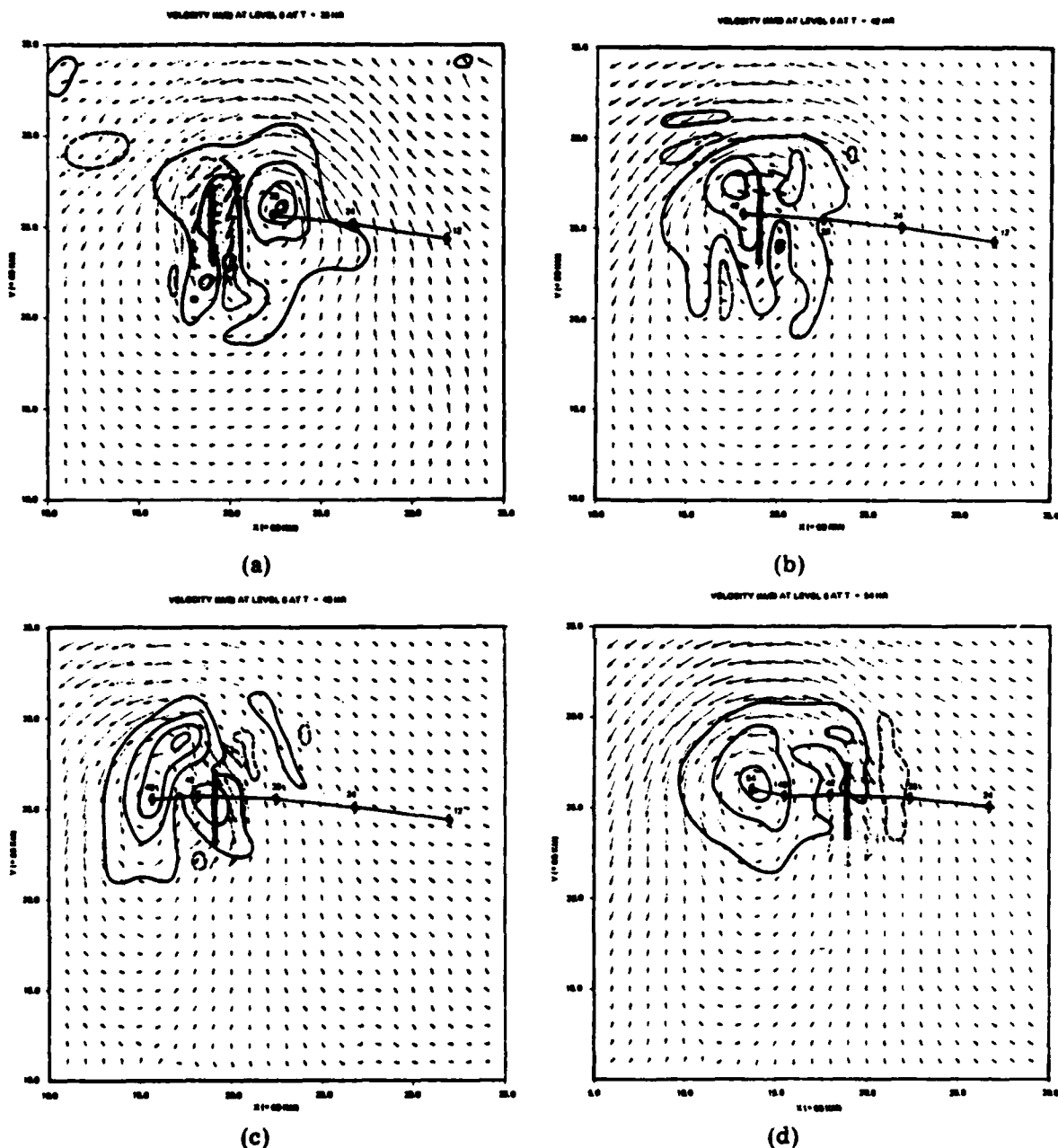
Fig. 5 — The 700-mb wind vectors, relative vorticity field, present and past center positions of Exp. 2 at (a) 36 h, (b) 42 h, (c) 48 h, and (d) 54 h. The values of the positive vorticities (solid) are 1, 2, 4, ... X 10^{-4} s^{-1}. The value of the negative vorticities (dash) are -1, -2, -3, ... X 10^{-4} s^{-1}.

32
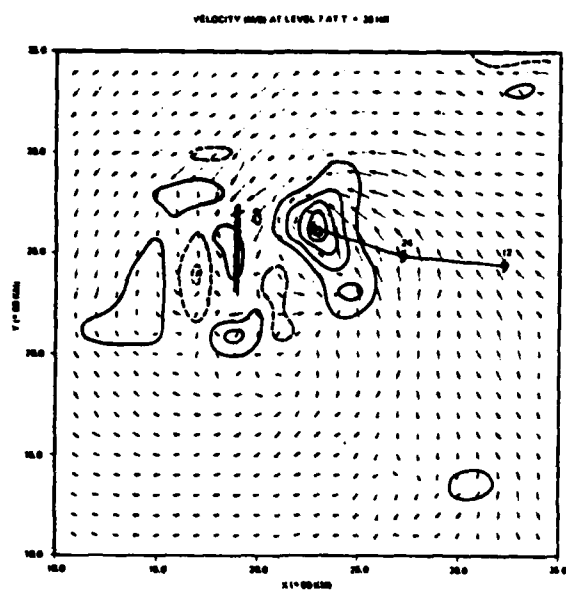
(a)
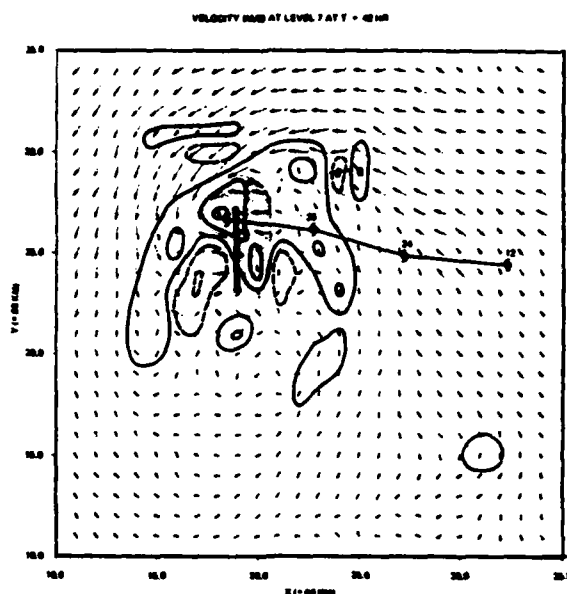
(b)
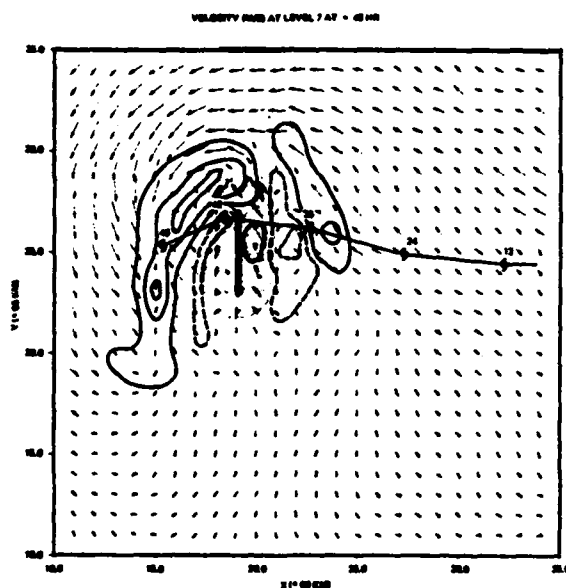
(c)
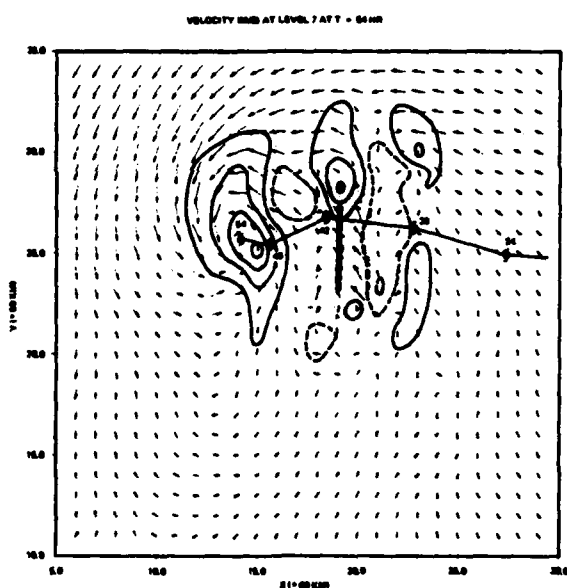
(d)

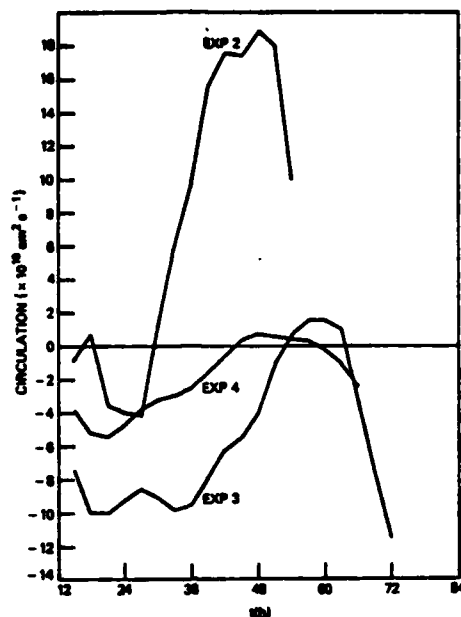Fig. 6 — Same as Fig. 5 except for the surface level ($\sigma = 0.965$)

Fig. 7 — The surface level circulation along a 480 × 640 km rectangular box
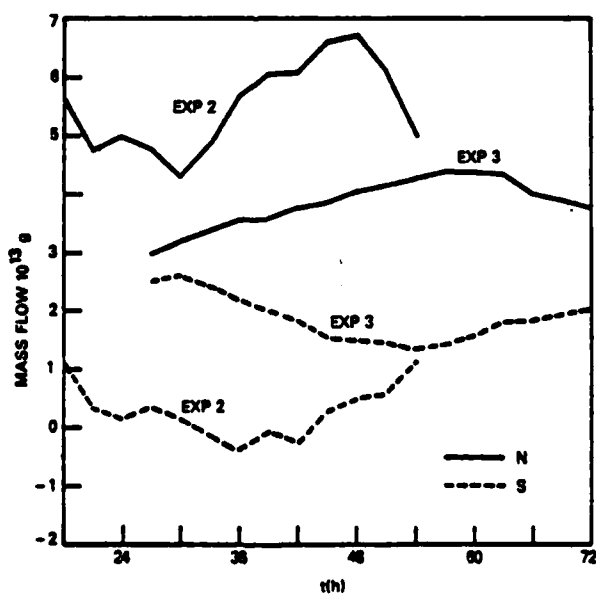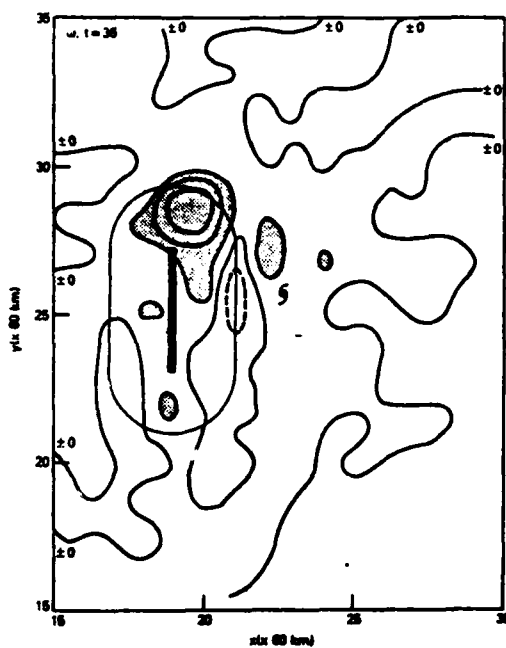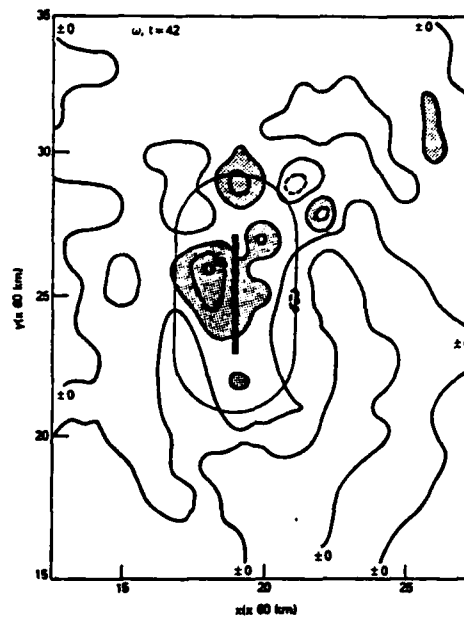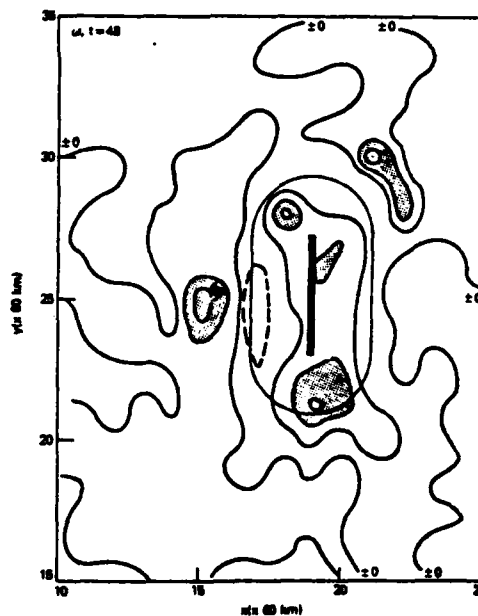centered around the ridge for Exps. 2, 3, and 4

Fig. 8 — The mass flow as defined by Eq. (5) of the northern (solid) cross-section
and southern (dash) cross-section for Exps. 3 and 3. Positive values denote cy-
clonic circulation; negative anticyclonic.

Fig. 9 — The vertical velocity at $\sigma = 0.93$ at (a) 36 h, (b) 42 h, and (c) 48 h. Contour intervals is 25 mb h^{-1}. Areas of upward motion stronger than -25 mb h^{-1} are shaded.
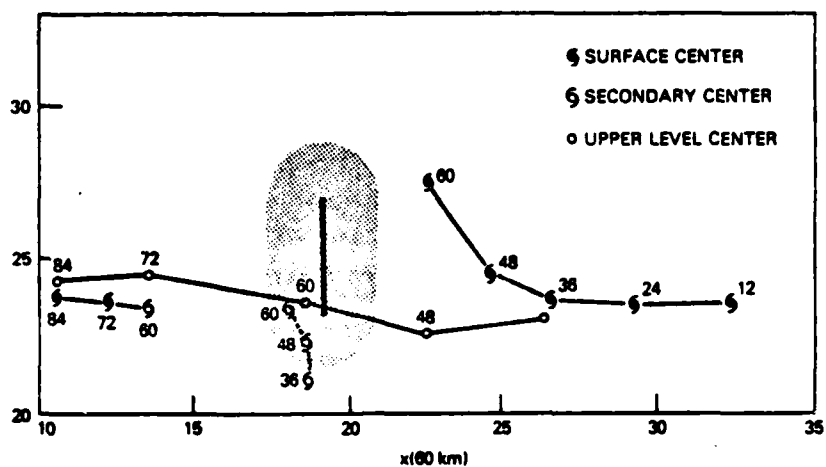
Fig. 10 — The movement of the surface (⚲) and 700-mb (o) centers for Exp. 3. The movements of secondary centers (⚲) are traced with a dashed line.
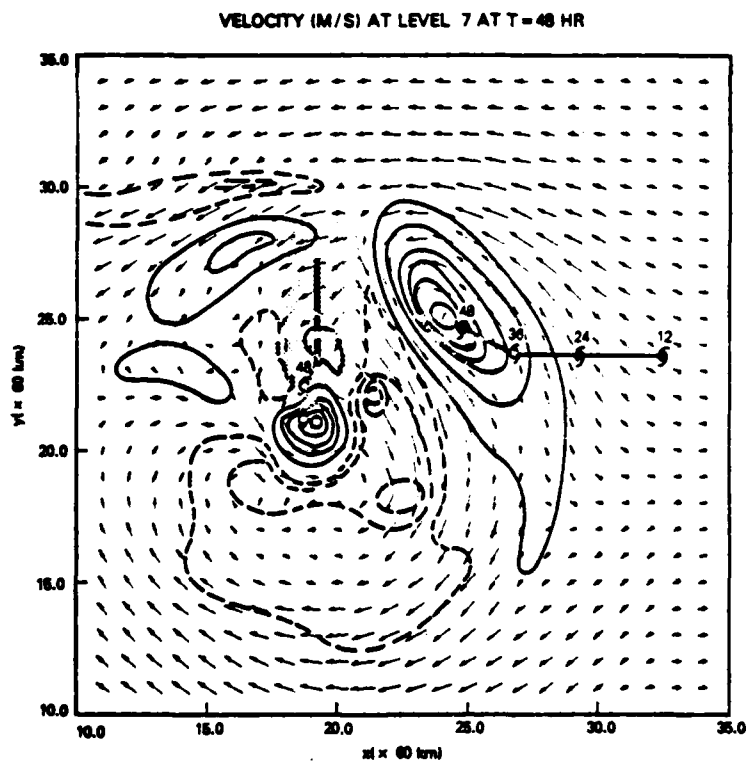

Fig. 11 — The surface wind vector and vorticity field at 48 h for Exp. 3 showing the deformation of the vortex and the strong anticyclonic flow around south of the mountain
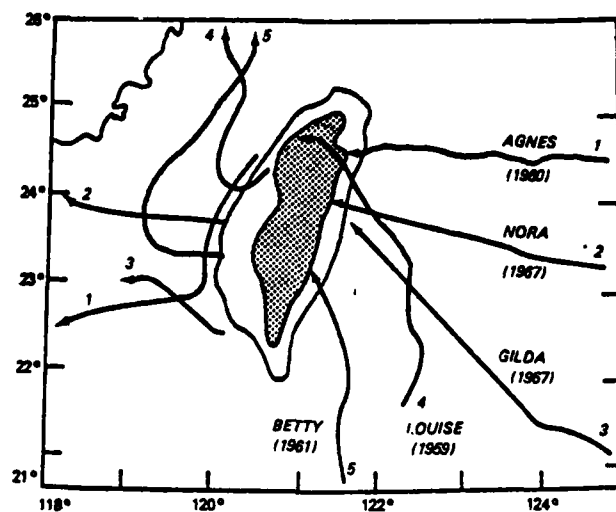
36

Fig. 12 — Paths of some weak typhoons that were prevented from passing the Central Mountain Range, and were replaced by the leeside secondary centers
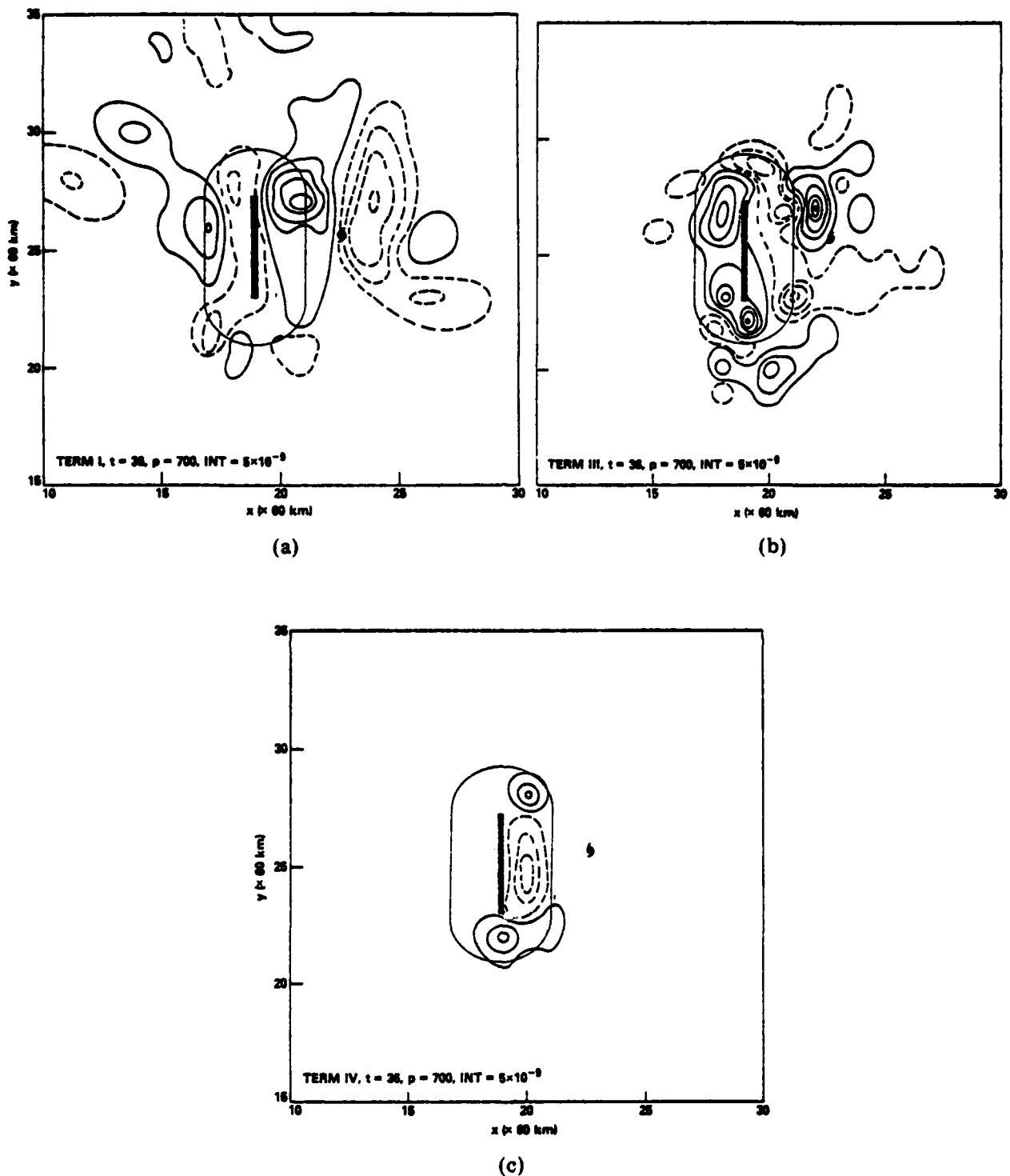
Fig. 13 — The spatial distributions of (a) horizontal advection, (b) divergence, and (c) twisting effects in the vorticity budget at 700-mb at 36 h for Exp. 2. Contour interval is 5×10^{-9} s^{-2}. Solid lines for positive values, dashed line for negative values.

APPENDIX

It is generally accepted that the intensity of simulated
tropical cyclones depends on the horizontal resolutions of the
numerical models. High horizontal resolutions near the center
are necessary to resolve the eye structure and strong pressure
gradient there. The high angular momentum in the inflow can also be
realized at small radii in models with high horizontal resolutions.
Rosenthal (1970) found differences in storm structure, kinetic
energy production, and rainfall rate even between a model with·
20-km resolution and another with 10-km resolution.

In order to show that the difference in the intensity
between our model tropical cyclone and that observed (Table 2)
is related to the 60-km resolution in our model, a set of supple-
mentary numerical experiments were carried out. The model
used is an axisymmetric analog to our three-dimensional model.
The initial condition, environmental stability, sea-surface
temperature, model physics are kept the same as the three-
dimensional model. Three integrations were performed with a 15-km
(Exp. A15), a 30-km (Exp. A30), and a 60-km (Exp. A60) resolution.
Quasi-steady states were reached in both experiments after 30 h.
A comparison of important storm parameters at 36 h is listed in
Table A1.

39

TABLE A1

Parameters	A15	A30	A60
Min. Pressure (mb)	941	945	973
Max. Wind Speed (m s^{-1})	66	57	34
Radius of Max. Wind (km)	45	60	120
Max. Rainfall Rate (cm day^{-1})	185	167	59
Max. Upward Velocity (cb h^{-1})	-65	-46	-19
Average Rainfall Within r = 120 km (cm day^{-1})	60	53	16
Conversion Rate from P.E. to K.E. within r = 300 km (10^{12} W)	4.0	5.5	3.3

There is clearly considerable differences among the three integrations. But the difference between A15 and A30 is smaller than that between A30 and A60. The stormy intensities of A15 and A30 are similar to those observed in typhoons (Wang, 1980), whereas the intensity of A60 is similar to our Exp. 2. The rate of P. E. conversion to K. E. in A15 within 300-km radius is smaller, because the storm in A15 is more concentrated.

These values suggest that a three-dimensional model with 15-km or 30-km resolution can produce a storm intensity comparable to those observed (Table 2) and that the coarse resolution in our three-dimensional model is responsible for the less intense tropical cyclone in Exp. 2. It is perhaps advisable to use a 30-km resolution in our three-dimensional model, but economic considerations dictated the 60-km resolution.

REFERENCES

Anthes, R. A., 1977: A cumulus parameterization scheme utilizing
a one-dimensional cloud model. Mon. Wea. Rev., 105, 270-286.

Arakawa, A. and V. R. Lamb, 1981: A potential enstrophy and energy
conserving scheme for the shallow water equations. Mon.
Wea. Rev., 109, 18-36.

Brand, S. and J. W. Blelloch, 1974: Changes in the characteristics
of typhoons crossing the island of Taiwan. Mon. Wea.
Rev., 102, 708-713.

Bussi, A. and S. Tibaldi, 1977: Inertial and frictional effects
on rotating stratified flow over topography. Quart. J. R.
Meteor. Soc., 103, 135-150.

Chang, C. C. and C. M. Chen, 1969: Laboratory modeling relevant
to hurricanes. Bull. Amer. Meteor., 50, 775-776.

Chang, S. W. 1981: Test of a planetary boundary layer parame-
terization based on a generalized similarity theory in
tropical cyclone models. Mon. Wea. Rev., 109, 843-853.

Chang, S. W. and R. V. Madala, 1980: Numerical simulation of the
influence of sea surface temperatures on translating
tropical cyclones. J. Atmos. Sci., 36, 2617-1630.

Chu, K. K., S. T. Wang, and H. P. Pao, 1977: Surface wind fields

    and moving tracks of typhoons when encountering the island

    of Taiwan. Conference Papers, 11th Tech. Conf. on Hurricanes

    and Tropical Meteorology, 13-16 Dec. 1977, Miami Beach, Florida,

    84-87. Available from Amer. Met. Soc., 45 Beacon Street,

    Boston, Mass. 02108.

Hayes, J. L. and R. T. Williams, 1977: Numerical simulations of

    air flow over mountains. Tech. Report NPS-63 Wu7741,

    Naval Postgraduate School, Monterey, California 93940.

Holton, J. R., 1979: An Introduction to Dynamic Meteorology.

    Academic Press, New York.

Madala, R. V., 1981: Efficient time integration schemes for atmosphere

    and ocean models, chapter 4, Finite-difference method for

    vectorized fluid dynamics calculations, Springer-Verlag Series

    in Computational Physics, D. L. Book, Editor.

Merkine, L., 1975: Steady finite-amplitude baroclines flow over

    long topography in a rotating stratified atmosphere.

    J. Atmos. Sci., 32, 1881-1893.

    _____ and E. Kalnay-Rivas, 1976: Rotating stratified flow

    over finite isolated topography. J. Atmos. Sci., 33, 908-922.

Pao, H. P. and R. R. Hwang, 1977: Effects of mountains on a
typhoon vortex: a laboratory experiment. Conference Papers,
11th Tech. Conf. on Hurricanes and Tropical Meteorology,
13-16 Dec. 1977, Miami Beach, Florida, 88-91. Available
from Amer. Met. Soc., 45 Beacon Street, Boston, Mass. 02108.

Rosenthal, S. L., 1970: Experiments with a numerical model of
tropical cyclone development: some effects of radial
resolution. Mon. Wea. Rev., 98, 106-120.

Sheets, R. C., 1969: Some mean hurricane soundings. J. Appl.
Meteor., 8, 134-146.

Smith, R. B., 1979: The influence of mountains on the atmosphere.
Advances in Geophysics, 21, 87-230, Academic Press,
New York.

Tibaldi, S., A. Bussi, and P. Malguzzi, 1980: Orographically
induced cyclogenesis: analysis of numerical experiments.
Mon. Wea. Rev., 108, 1302-13-4.

Wang, S. T., 1980: Prediction of the behavior and strength of
typhoons in Taiwan and its vicinity (in Chinese). Research
Report 108, Chinese National Science Council, Taipei, Taiwan.
Available from the author at Central Weather Bureau,
64 Kung-Yuan Road, Taipei, Taiwan.

Wei, D. W., 1979: Studies on tropical storm by experimental

    simulation in the laboratory. Preprint, International

    Conference on Tropical Cyclones, 25-29 Dec. 1979, Royal

    Meteorological Society (Australia Branch), Perth. c/o Dept.

    of Physics, Western Australia Institute of Technology,

    Hayman Road, Bentley, 6102, Australia.

Yamada, T., 1976: On the similarity functions A, B, and C of the

    planetary boundary layer. J. Atmos. Sci., 33, 781-793.